

Induced apoptosis against U937 cancer cells by Fe(II), Co(III) and Ni(II) complexes with a pyrazine-thiazole ligand: Synthesis, structure and biological evaluation

Pradip Bera^{a,1}, Abhishek Aher^b, Paula Brandao^c, Sunil Kumar Manna^{b,*}, Gopinath Mondal^a, Abhimanyu Jana^a, Ananyakumari Santra^a, Harekrishna Jana^d, Pulakesh Bera^{a,*}

^a Department of Chemistry, Panskura Banamali College (Vidyasagar University), Panskura R.S, Midnapore (East), West Bengal 721152, India

^b Centre for DNA Fingerprinting & Diagnostics (CDFD), Hyderabad, Telangana 500 039, India

^c Department of Chemistry, CICECO, University of Aveiro, 3810-193 Aveiro, Portugal

^d Department of Microbiology, Raja Narendralal Khan Womens' College (Vidyasagar University), Midnapore (West), West Bengal 721152, India

ARTICLE INFO

Article history:

Received 6 January 2020

Accepted 26 February 2020

Available online 8 March 2020

Keywords:

Pyrazine thiazole
Iron(II) complex
Cobalt(III) complex
Nickel(II) complex
Cytotoxicity
DNA binding

ABSTRACT

Complexes of iron(II), cobalt(III) and nickel(II) with 4-(4-methoxyphenyl)-2-(2-(1-(pyrazin-2yl)ethylidene)hydrazinyl)thiazole (PyztH) have been synthesized and characterized by elemental analyses, spectroscopic methods, CV measurements and a DFT study. The crystal and molecular structures were determined by the X-ray diffraction method. The complexes have the compositions [Fe(Pyzt)₂]Br₂ (**1**), [Co(Pyzt)₂]PF₆ (**2**) and [Ni(Pyzt)(PyztH)]ClO₄ (**3**), with an approximate octahedral environment around the metal centre with NNN donor atoms from the two coordinating ligands. The complexes belong to the triclinic crystal system and crystallize in the space group *P*-1. Complex **1** is stabilized by strong hydrogen bonds, whereas the stability of complexes **2** and **3** is associated to π - π stacking interactions. The chemical reactivity, frontier orbital picture and energies of the HOMO and LUMO of the complexes have been estimated by a DFT study. The complexes are redox active species and respond with a quasi-reversible redox process. The cytotoxicity of the complexes was tested against U-937 human monocytic cells and shows IC₅₀ values of 132 (for **1**), 45 (for **2**) and 162 μ M (for **3**). A LDH release assay indicates that **2** and **3** show apoptosis in the tumour cell. Complex **2** induces apoptosis by disrupting the mitochondrial membrane potential and homeostasis leading to cytotoxicity, as envisaged by PARP cleavage. Complexes **1**, **2** and **3** show high binding constants ($2.01 \times 10^6 \text{ M}^{-1}$ for **1**, $1.18 \times 10^7 \text{ M}^{-1}$ for **2** and $2.90 \times 10^7 \text{ M}^{-1}$ for **3**) with CTDNA which attest the groove binding nature of the complexes with DNA. The compounds also exhibit a remarkable zone of inhibition against specific tested bacterial and fungal strains. Based on the results, the cobalt complex (**2**) shows the best antitumor and antimicrobial activity among the complexes under investigation.

© 2020 Elsevier Ltd. All rights reserved.

1. Introduction

Nitrogen and sulfur containing heterocyclic compounds occur in nature in the form of alkaloids, vitamins, pigment and as constituents of animal and plant cells. Thiazole is a well known stable nitrogen and sulfur containing heterocyclic aromatic compound, having a Bird's Index of Aromaticity value of 79 [1]. It possesses both an electron-accepting function (i.e., $-\text{C}=\text{N}-$) and an electron donating atom ($-\text{S}-$) [2]. The presence of an acidic proton at the C2 atom is responsible for the high reactivity of the thiazole ring

[2]. Various new biochemical entities have been generated using the thiazole moiety as a synthon. Different groups substituted on the thiazoles rings at various positions (Fig. 1) lead to a variety of thiazoles containing compounds which have wide applications in biology and pharmacy [3–6].

Biological activities, like antihypertensive, anti-inflammatory, antibacterial, antiHIV, antitumor and cytotoxic activities, were reported for thiazole lead compounds [7–11]. Some synthetic drugs, like fanetizole (anti-inflammatory agent), tiazofurin (anti-neoplastic agent), penicillin (potent antibiotic), sulfatiazol (antimicrobial) and abafungin (antifungal), possess thiazole rings [12–14]. Penicillin is a known naturally occurring antibiotic where thiazolidine is the core unit [15]. Thiazole and thiophen based heterocyclic compounds were reported as antitumor agents towards

* Corresponding authors.

¹ Present address: Department of Chemistry, Kandi Raj College, Murshidabad, West Bengal 742137, India.

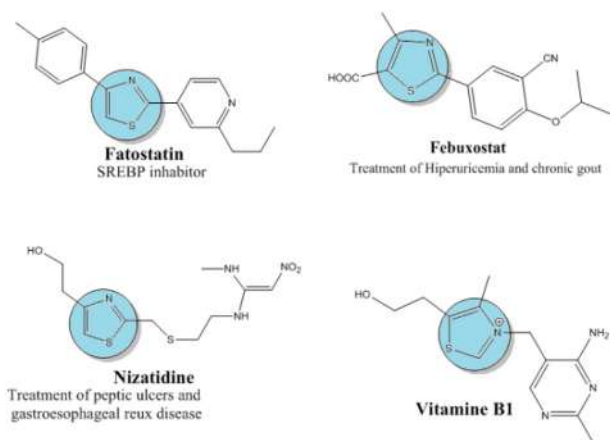


Fig 1. Illustrative examples of bioactive substituted thiazole compounds.

the human gastric cancer (NUGC and HR), human colon cancer (DLD1), human liver cancer (HA22T and HEPG2), human breast cancer (MCF) and nasopharyngeal carcinoma (HONE1) cell lines [16–19]. Additionally, photochemical isomerisation of thiazole plays an important role in many applications and has been studied in detail [20]. 2,4-Di-substituted multiple donor thiazole-based compounds were recommended as a ligand in biochemistry due their ability to coordinate with various metal ions. The complexes are shown to be active agents towards various bacteria and fungi. More et al. have synthesized a series of multiple donor thiazole Schiff base ligands exhibiting anti-bacterial and anti-biofilm activity against *B. subtilis* and *E. coli*. A novel anti-inflammatory agent like Darbufelone (CI-1004) and the methane sulfonate salt also have a thiazole core unit [21]. A number of 2,4 di-substituted pyridine thiazole compounds, like (4-(4-methoxy phenyl)-2-(2-(1-pyridine-2-yl)ethylidene)hydrazinyl)thiazole, show anti-cancer activity against human breast cancer MCF-7. Similar compounds were also found to be potential antibacterial agents against both gram positive and gram negative bacteria [8,22]. Benoit Bertrand et al. first reported a pyrazine-based imidazole Au(III) complex which has respectable antiproliferative properties against the HL60 leukemia cell and acts as an anticancer agent against HL60, MCF-7 (breast cancer), A5499 (Human adenocarcinoma lung cancer) and MRC-5 (human lung fibroblasts) cells [23]. Generally, thiazole-pyrazine ligands and their metal complexes are a class of heterocyclic compounds which possess a wide range of biological and catalytic properties. Li et al. have extensively investigated a thiosemicarbazone derivative of 2-acetylpyrazine as a potential anticancer agent [24,25]. Jonas Bostrom et al. also reported a novel class of thiazole-pyrazine compounds as cannabinoid (CBI) receptor antagonists for the treatment of obesity [26]. In this study, we report the synthesis and structure of a new ligand (PyztH) and its metal complexes. The anticancer activity against U-937 (human blood cancer cell) and the interactions of the molecules with CT-DNA are investigated.

2. Experimental

2.1. Materials and methods

Thiosemicarbazide (99%), 2-acetyl pyrazine (99%) and 2-bromo-4-methoxyacetophenone were obtained from Aldrich chemical company. Ferrous nitrate hexahydrate, nickel nitrate hexahydrate, cobalt perchlorate hexahydrate and ammonium hexafluoro phosphate were obtained from Merck chemical company. All solvents were obtained from commercial suppliers and used after distillation.

2.2. Synthesis of the ligand 4-(4-methoxyphenyl)-2-(2-(1-(pyrazine-2-yl)ethylidene)hydrazinyl)thiazole (PyztH)

The present ligand (PyztH) was prepared by the condensation of 2-bromo-1-(4-methoxyphenyl)ethen-1-one and 2-(1-(pyrazine-2-yl)ethylidene)hydrazine-1-carbothioamide. An anhydrous methanolic solution of 2-bromo-1-(4-methoxyphenyl)ethen-1-one (10 mmol) was added dropwise to a methanolic solution (20 mL) of 2-(1-(pyrazine-2-yl)ethylidene)hydrazine carbothioamide (10 mmol, 1.942 g) with constant stirring at RT. After the complete addition, the reaction mixture was refluxed in a water bath for three hours. An orange yellow precipitate was obtained, which was filtered off and washed 2 to 3 times with aqueous methanol. The crude product was recrystallized with a methanol and acetonitrile mixture. A light orange transparent micro-crystalline product was obtained by diffusion of methanol into the mixture. Yield: 3.124 g (73.79%). M.P. (decomposition temperature): 170 °C. Anal. Calc. for $C_{16}H_{16}BrN_4O_2S$ (%): C, 48.35; H, 4.30; N, 13.27; Found C, 48.19; H, 4.48; N, 13.22; IR (KBr pellets, cm^{-1}): ν_{N-H} 3446, $\nu_{azomethen (C=N)}$ 1606, $\nu_{thiazole (C=N)}$ 1501, $\nu_{(C-O)}$ 1247, $\nu_{(C-S)}$ 825. 1H NMR ($CDCl_3$), δ (ppm): 2.37–2.49, (s, 3H at C6), 3.77 (s, 3H at C16), 6.96 and 6.98 (d, 2H at C12 and C14, $^3J_{13,12} = ^3J_{14,15} = 8.0$ Hz); 7.25 (s, 1H at C8), 7.80 and 7.82 (d, 2H at C11 and C15, $^3J_{12,14} = ^3J_{11,15} = 8.0$ Hz), 9.20 (s, 1H at C3), 8.56–8.61 (d, 2H at C1 and C2).

2.3. Synthesis of the complex $[Fe(Pyzt)_2]Br_2$ (1)

A methanolic solution of $Fe(NO_3)_2 \cdot 6H_2O$ (0.57 g, 2.0 mmol) was added drop by drop to a 30 mL of methanol:acetonitrile (2:1) solution of PyztH (0.77 g, 2.0 mmol) with constant stirring. The resulting solution was refluxed at 80 °C for 4 h under an N_2 atmosphere. The colour of the solution changed from yellow to dark brown. The reaction mixture was filtered and placed in a 50 mL vacuum desiccator. Green transparent crystals were obtained upon slow evaporation. The solid crystalline product was collected by filtration and washed with an acetonitrile–methanol mixture. Yield 75% (with respect to the metal salt). Anal. Calc. for $C_{32}H_{30}Br_2FeN_{10}O_2S_2Br_2$ (%): C, 44.36; H, 3.49; N, 16.17. Found C, 43.51; H, 3.62; N, 15.86. IR (KBr pellets, cm^{-1}): $\nu_{(N-H)}$ 3436, $\nu_{(C-O)}$ 1268, $\nu_{(C-S)}$ 832, $\nu_{(N-H)}$ 618.

2.4. Synthesis of the complex $Co[(Pyzt)_2]PF_6$ (2)

A mixture of $Co(NO_3)_2 \cdot 6H_2O$ (0.58 g, 2.0 mmol) and PyztH (0.77 g, 2.0 mmol) were stirred in mixture of 20 mL methanol and 10 mL acetonitrile, followed by addition of a 5 mL aqueous solution of ammonium hexafluoro phosphate (0.65 g, 4.0 mmol) with constant stirring. The stirring was continued for 2 h at 80 °C whereupon the colour of the solution changed to deep wine red. The reaction mixture was then filtered and dark brown microcrystals of 2 separated out from the solution upon standing at ambient temperature. Analytically pure dark brown crystals suitable for X-ray diffraction were obtained from the acetonitrile solution of the crude product. Yield 72% (with respect to the metal salt). Anal. Calc. for $C_{32}H_{28}CoF_6N_{10}O_2PS_2$ (%): C, 44.97; H, 3.54; N, 16.39; S, 7.50. Found C, 45.03; H, 3.28; N, 16.4; S, 7.52. IR (KBr pellets, cm^{-1}): $\nu_{(C=N)}$ 1400, $\nu_{(C-O)}$ 1245, $\nu_{(P-F)}$ 1083, $\nu_{(C-S)}$ 835.

2.5. Synthesis of the complex $[Ni(Pyzt)(PyztH)]ClO_4$ (3)

A 10 mL methanolic solution of $Ni(ClO_4)_2 \cdot 6H_2O$ (0.25 g, 1.0 mmol) was added drop by drop to a solution (10 mL methanol, 10 mL acetonitrile and 1 mL DMF) of PyztH (0.38 g, 1.0 mmol). The resulting solution was stirring at 80 °C for 1 h, during which time the mixture turned from orange yellow to a deep red colour. The

stirring was continued at this temperature for another three hours. The reaction mixture was filtered. Dark brown rod-shaped crystals separated out from the solution upon slow evaporation. Yield 68% (with respect to the metal salt). Anal. Calc. for $C_{32}H_{30}ClN_{10}NiO_6S_2$ (%): C, 47.51; H, 3.74; N, 17.32; S, 7.93. Found C, 47.43; H, 3.71; N, 17.35; S, 7.93. IR (KBr pellets, cm^{-1}): $\nu_{(azomethine\ C=N)}$ 1602, $\nu_{(C=N)}$ 1492, $\nu_{(C-O)}$ 1243, $\nu_{(C-S)}$ 824, $\nu_{(Cl-O)}$ 618.

2.6. Instrumentation and methods

A Perkin Elmer Lambda 35 spectrophotometer with a wavelength range 200–800 nm was used to evaluate the UV–Vis absorption spectra of the ligand and the complexes at room temperature. FT-Infrared spectra of the samples were recorded in the range 4000–500 cm^{-1} using a Perkin Elmer Spectrum spectrophotometer with the samples prepared as KBr plates. The elemental analysis (C, H, N and S) both the ligand and the complexes was performed using a FISON EA-1108 CHN analyzer. The single crystal X-ray diffraction data were collected on a Bruker APEX II CCD diffractometer at 150 K using graphite-monochromatic Mo- K_{α} radiation (0.71073 Å). The data were processed and corrected for absorption as well as for Lorentz and polarization effects. All structures were solved by intrinsic phasing with SHELXT [27] and further refined by full matrix least squares with SHELXL [28]. All non-hydrogen atoms had anisotropic thermal parameters. Hydrogen atoms were included in the structure factor calculations in geometrically idealized positions with isotropic thermal displacements depending on the parent atom, using a riding model. A summary of the crystallographic data and refinement parameters is given in Table 1. The molar conductance of 10^{-3} (M) solutions of the metal complexes in dry acetonitrile were measured at 30 °C using a Thermo Orion model 550A conductivity meter and a dip-type cell with a platinum electrode.

2.7. DFT calculations

HOMO and LUMO orbitals were plotted using the X-ray coordinates of the complexes. The ground state electronic structure of the complexes was calculated using the DFT method [29] with the Orca 4.0 program. Becke's hybrid function [30,31] with the Lee-Yang-Parr (LYP) correlation function [29] was used throughout the study. The valence only SV (P) SV/J basis set and B3LYP/G effective one potential functional were used [32]. All energy calculations were performed using the self-consistent field "tight" option of the Orca 4.0.1 program to ensure sufficiently well converged values for the state energies.

2.8. In vitro biological studies

2.8.1. Cytotoxicity assay

The cell cytotoxicities of the complexes were evaluated by an MTT, 3-(4,5-dimethylthiazol-2-yl)-2,5-diphenyltetrazolium bromide, assay based on the ability of mitochondrial dehydrogenase in the viable cells to leach the tetrazolium rings of MTT. Dark blue membrane-impermeable formazan crystals are obtained, which are measured spectrophotometrically. The formazan gives a measurement of the number of viable cells. About 5000 cells/well of human histiocytic lymphoma U-937 were seeded in a 96 well plate and incubated for 30 min. The cells were then treated with 0.75–100 μM of **PyztH**, **2**, **3** and **1**. After 72 h of incubation in a 5% CO_2 incubator at 37 °C, 10 μL of MTT dye (4 mg/mL in PBS) was added to each well and the incubation was continued for 3 h at 37 °C. To solubilize the cell membrane, 100 μL of lysis buffer (20% SDS in 50% dimethylformamide) was added in the culture medium and it was kept on a shaking rocker (200 rpm) overnight to dissolve the formazan crystals completely. The absorbance was taken at 595 nm

Table 1

UV–vis absorbance in CH_3OH and fluorescence spectroscopy in $CH_3OH + DMSO$ (1:2).

Compounds	λ_{max} 1(absorption) in nm ($\epsilon \times 10^{-5}/M^{-1}cm^{-1}$)	Assignments	$\lambda_{emission}$ (λ_{ex}) nm
PyztH	284 (0.603) 370 (0.240)	$\pi \rightarrow \pi^*$ $n \rightarrow \pi^*$	713 (3 7 0)
1	275 (0.497) 358 (0.299) 441 (0.154) 639 (0.022)	$\pi \rightarrow \pi^*$ $n \rightarrow \pi^*$ MLCT $T_{2g} \rightarrow E_g$	813 (3 8 0)
2	373 (0.184) 507 (0.219)	$n \rightarrow \pi^*$ MLCT	814 (3 9 0)
3	380 (0.131) 505 (0.117)	$n \rightarrow \pi^*$ MLCT	768 (3 8 0)

using a BIO-RAD iMark Microplate Reader with a Microplate Analyt. The IC₅₀ values were determined by non-linear regression analysis using Graph Pad Prism software [33].

2.8.2. Lactate dehydrogenase (LDH) release assay

LDH, a cytosolic enzyme, is released into a culture supernatant upon induction of necrosis of cells. U-937 cells (2×10^6) were taken per well in a 6-well plate. After a brief incubation of 30 min, the cells were treated with compounds **PyztH**, **2**, **3** and **1** at the IC₅₀ concentration for 6 h and 24 h. The culture supernatants were isolated and 0.1 mL of LDH Mix (2.8 mL of 0.2 M Tris-HCl, pH 7.3; 0.1 mL of 6.6 mM NADH and 0.1 mL of 30 mM sodium pyruvate) was added to each well. The absorbance was taken at 340 nm, 25 °C and at 5 min intervals for a period of 30 min using Spectramax M5 by Molecular Devices and Softmax pro 7.0 software. A graph was plotted to calculate the LDH release. The LDH activity was indicated as relative cytolysis of the compound treated cells from a plot considering absorbance of Triton X-100 treated cells as 100% [34].

2.8.3. PARP cleavage by western blot

U-937 cells (2×10^6) were seeded into each well of two 6 well plates. The plates were treated for 24 h with 25 μM and 50 μM of each of **PyztH**, **2**, **3** and **1**, and Doxorubicin (3 μM) at 37 °C in a 5% CO_2 incubator. The cells were centrifuged and the supernatant was discarded. The cells were lysed by adding 50 μL of lysis buffer [Tris-HCl, 50 mM, pH 8; NaCl, 150 mM; EGTA, 1 mM; Nonidet P-40, 0.5%; sodium deoxycholate, 0.25%; $1 \times$ protease arrest cocktail (G-Biosciences, Cat 786-437)] followed by intermediate vortexing for 30 sec and subsequently incubating on ice for 30 s. This is continued for 45 min. The cell lysate supernatant was used. $6 \times$ SDS loading dye was added accordingly to the supernatant. This was boiled at 100 °C for 5 min and then allowed to cool. The cell lysate was resolved on 10% SDS-polyacrylamide gel. The gel was run at 90 V for 2 h (until the dye front got out of the gel). The gel was then electro-transferred onto an activated PVDF membrane via a wet transfer method. The PVDF membrane was incubated in 5% fat-free milk (0.5 g dry milk and 10 mL TBST) for 45 min. The membrane was blotted with 1:5000 dilution of the cleaved PARP (Asp214) (Cell Signaling Technology, Cat D64E10) primary antibody raised in a rabbit. This was incubated overnight at 4 °C. After washing 3 times with TBST, the blot was incubated with the HRP-conjugated secondary antibody (anti-Rabbit IgG raised in a goat) in 1:7000 dilutions. This was incubated for 45 min at RT. Three TBST washes were then given. Signals were detected using a chemi-luminescent substrate (femto LUCENT PLUS-HRP, G-Biosciences) [35]. The results were visualized under UVITEC Chemidoc (Cambridge), using UVITEC Nine Alliance software.

2.8.4. Cytotoxicity assay for peripheral blood mononuclear cells (PBMC)

PBMCs were isolated using Ficoll-Histopaque. Briefly, 4 mL of blood was layered on 4 mL of histopaque (1.077), keeping both layers separate in a 15 mL centrifuge tube. The tube was centrifuged (without any delay) for 30 min at 100g at room temperature. On aspirating, a whitish buffy coat layer (about 1 mL) (PBMCs) formed in the interphase between histopaque and the medium. The PBMCs were washed with PBS and saline. About 5000 cells/well of PBMCs were seeded in a 96 well plate and after 30 min of incubation, were treated with IC₅₀ and double IC₅₀ concentrations of **PyztH**, **2**, **3** and **1**. After 24 h of incubation in a 5% CO₂ incubator at 37 °C, 10 μL of MTT dye (4 mg/mL in PBS) was added per well and they were further incubated for 3 h at 37 °C. Later, 100 μL of lysis buffer (20% SDS in 50% dimethyl formamide) was added to the culture medium and kept on a shaking rocker (200 rpm) overnight in the dark to solubilize the cell membrane and dissolve the formazan crystals [36]. The absorbance was taken at 595 nm and the cell death was calculated from the data as mentioned before.

2.8.5. Docking study

Molecular docking was carried out using AUTODOCK 4.0 software with the graphical user interface AUTODOCK TOOLS 4.0 (AD4.1_bound.dat) [37,38]. The macro cyclic receptor was chosen to be PDB, formed with the three dimensional X-ray crystal structure of Focal Adhesion Kinase (FAK) (entry 6cb0 in the Protein Data Bank).

The graphical user interface AUTODOCK TOOLS is devoted to the protein setup; water molecules are deleted from the crystal structure of the protein and only polar hydrogen atoms are added. The computed Gasteigers charge was calculated as -2.9878 kcal/mol and non-polar hydrogen atoms were merged to the carbon atoms. The 3D structures of the complexes were saved in PDB format, with the aid of the program MERCURY. The AUTODOCK TOOLS program was used to make a docking input file. The grid box size for complex **1–3** are 86 × 94 × 96, 82 × 96 × 94 and 92 × 92 × 92, respectively, with a grid spacing of 1 Å. Both the receptor and complexes are save in the pdbqt format. A distance-dependent function of the dielectric constant was used for the calculation of the energetic map. Ten runs were generated using Lamarckian genetic algorithm searches. The default settings were used with an initial population of 50 randomly placed individuals and a maximum number of 2.5 × 10⁶ energy evaluations [39]. The final docking was run with the autogrid4.exe and autodock4.exe functions to generate glg and dlg files respectively. The Dlg file was analysed with autodock Tools software. Finally, the written complex was saved in the PDB format. The graphical interaction pictures were found using the PDB file with Schrodinger software.

3. Results and discussion

A new ligand, PyztH, was synthesized by the reaction of (E)-2-(1-(pyrazin-2-yl)ethylidene)hydrazine-1-carbothioamide and 2-bromo-4-methoxyacetophenone in methanol. Fe(NO₃)₂·6H₂O, Co(NO₃)₂·6H₂O and Ni(ClO₄)₂·6H₂O produce complexes with the compositions [Fe(Pyzt)₂]Br₂, Co(Pyzt)₂]PF₆ and [Ni(Pyzt)(PyztH)]ClO₄, respectively when each salt was refluxed with two equivalent of PyztH in a methanol-acetonitrile mixture.

3.1. Spectral study

3.1.1. ¹H NMR and FTIR studies

The signals obtained in the ¹H NMR spectrum of **PyztH** (Fig. S1) are in good agreement with the expected structure. The signal at δ 2.37–2.49 ppm can be assigned to the three iminomethyl protons

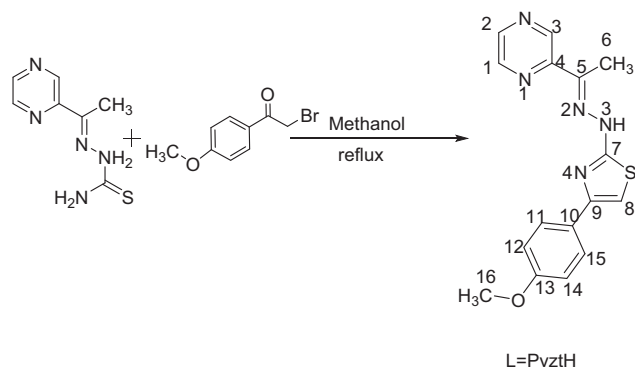
at C6. Another singlet peak was observed at δ 7.25 ppm for the single H atom at C8. The doublet peak in the region δ 6.98 ppm can be assigned to the protons attached to C12 and C14, with a J value of 8.0 Hz (Scheme 1). Similarly, the doublet peak in the region δ 7.80–7.82 ppm corresponds to the protons attached to C11 and C15, respectively, with a J value of 8.0 Hz. The J values indicate that the protons attached to C11 and C12 mutually couple to the same extent as the coupling of protons attached to C14 and C15.

The IR spectrum of the ligand (Fig. S2) shows a low intense broad band at 3461 cm⁻¹ due to the hydrazone (-NH) bond. Another high intense sharp band at 1606 cm⁻¹ is attributed to the azomethine (C=N) vibration and another high intense band is observed at 1501 cm⁻¹ due to the vibration of the C=N bond (thiazole ring). Low intense stretching frequencies at 1247 and 825 cm⁻¹ indicate the presence of -CO- (phenoxy) and -CS- (thiazole ring) bonds, respectively [20]. In order to study the coordination mode of the ligand with the metal ions, the IR spectrum of the free ligand was compared with the spectra of the complexes. In **1** (Fig. S3), a low intense broad band at 3463 cm⁻¹ is observed due to the NH bond of the ligand. The ν_{C-O} (phenoxy) and ν_{C-S} (thiazole) bond vibrations remain unchanged upon complex formation. A high intense band at a lower frequency, 518 cm⁻¹, is due to internal hydrogen bond vibrations present in the complex. In **2** (Fig. S4), shifting of the ν_{C=N} (thiazole) peak (1400 cm⁻¹ in the ligand) to the lower frequency side by about 100 cm⁻¹ indicates the involvement of the thiazole ring nitrogen atom in coordination [22]. A low intense lower region band at 1083 cm⁻¹ is attributed to the presence of the uncoordinated counter anion PF₆⁻ [40]. In complex **3** (Fig. S5), the shifting of the ν_{C=N} (azomethine; 1602 cm⁻¹) and ν_{C=N} (thiazole ring; 1492 cm⁻¹) bands to a lower frequency range by 4–10 cm⁻¹ on complexation is attributed to coordination through the azomethine and thiazole ring nitrogen atoms to the Ni²⁺ ion. The stretching vibration at 618 cm⁻¹ is due to the perchlorate anion.

3.1.2. UV-visible and fluorescence spectral studies

Electronic spectral measurements are helpful in assigning the stereochemistry of the central metal ion in complexes, based on the positions, intensity and number of d-d transition peaks. The electronic absorption spectra of **PyztH**, **1**, **2** and **3** in CH₃OH solution (10⁻⁶ M) at room temperature are shown in Fig. 2. The high energy bands in the range 284–373 nm could be attributed to spin allowed π → π* transitions in the ligand moiety, while the low intensity bands in the range 441–507 nm could be assigned as MLCT (d_M → Pyzt) (Table 1).

The electronic spectrum of **PyztH** shows two absorption bands at 284 and 370 nm (Fig. 2). The low energy band at 370 nm corresponds to the n → π or π → π* electron transition from the HOMO to the LUMO. The absorption spectrum of **1** shows three absorption



Scheme 1. Ligand preparation with labelling of the C atoms

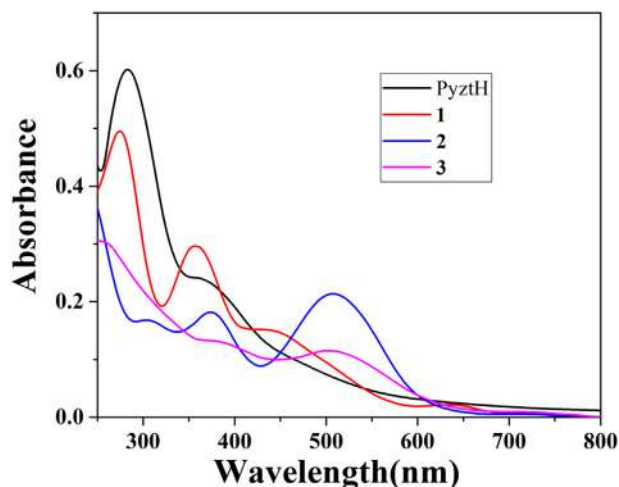


Fig 2. UV-vis spectra of PzvtH, **1**, **2** and **3** in CH₃OH solution at 10⁻⁵ M concentration.

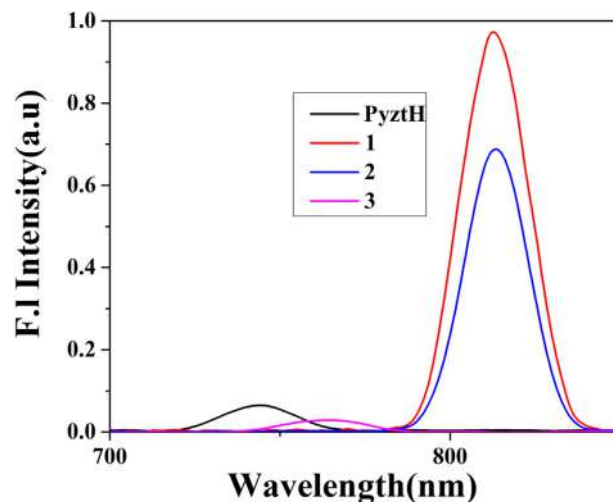
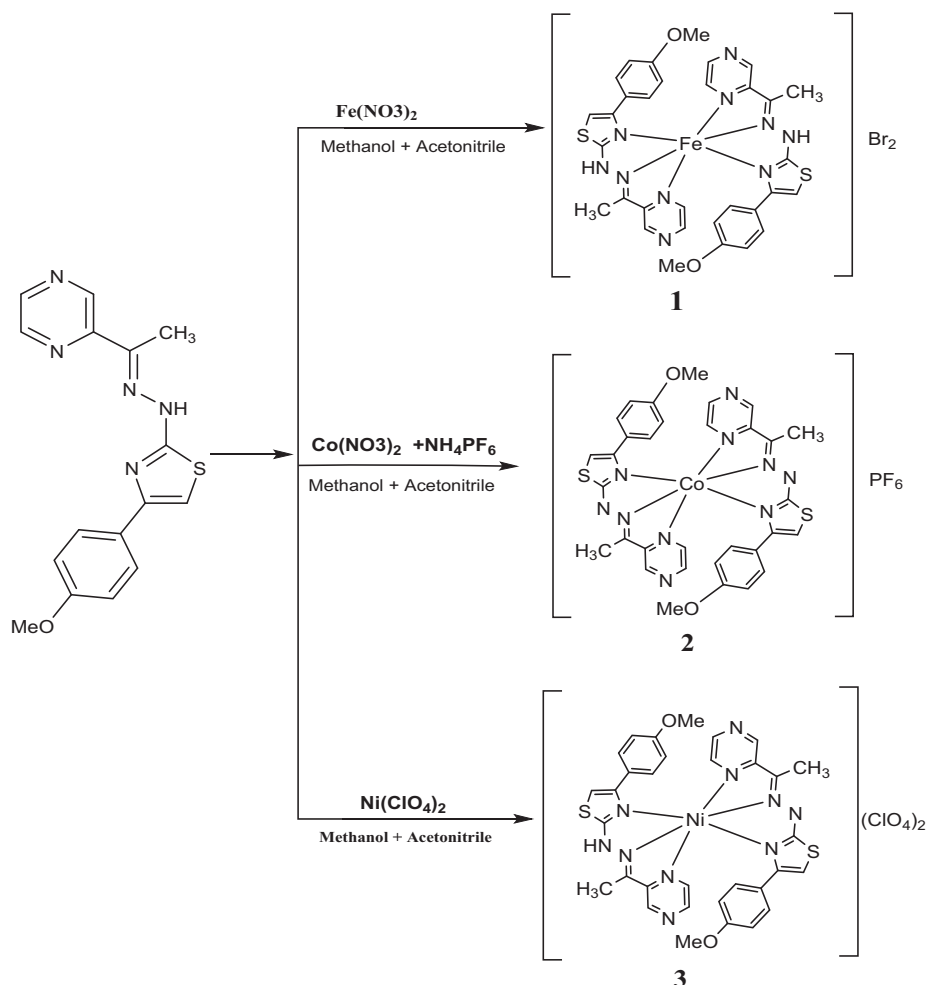


Fig 3. Fluorescence intensity of PzvtH and complexes **1**, **2** and **3**.

bands at 639, 441 and 358 nm, corresponding to $T_{2g} \rightarrow E_g$, $M \rightarrow L$ charge transfer (MLCT) and $n \rightarrow \pi^*$ or $\pi \rightarrow \pi^*$ electron transitions in the coordinated ligand, respectively. Similarly for **2**, the observed higher energy peaks at 373 and 507 nm can be assigned to $n \rightarrow \pi^*$ or $\pi \rightarrow \pi^*$ electron transitions of the coordinated ligand and a MLCT transition, respectively. In **3**, the absorption bands at

380 and 505 nm are due to a $n \rightarrow \pi^*$ or $\pi \rightarrow \pi^*$ electron transition of the coordinated ligand and a MLCT transition, respectively. The UV absorption spectra prove the partial covalent nature of the M-L bond. The HOMO and LUMO molecular orbital picture from single point DFT measurements of all the complexes also proved the maximum electron density on ligand's orbital (*vide infra*), which sup-



Scheme 2. Synthesis of **1**, **2** and **3**.

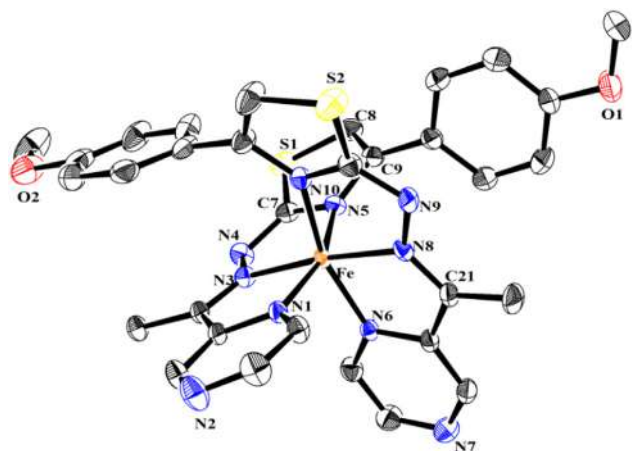


Fig 4. Molecular structure of **1**. Thermal ellipsoids are drawn at the 50% probability label. For the clarity of the structure, hydrogen atoms have been omitted. The structure is truncated to highlight the ligand–metal binding geometry.

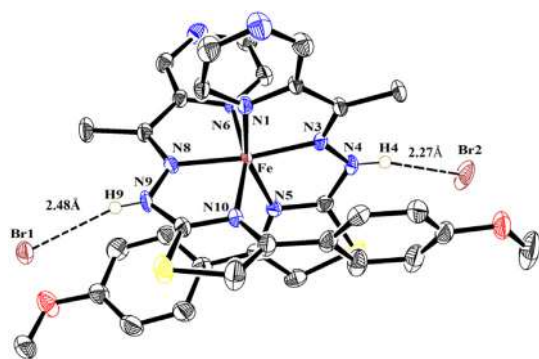


Fig 5. Hydrogen bonding interactions in **1**.

ports the $n \rightarrow \pi^*$ or $\pi \rightarrow \pi^*$ electron transition in the optimized structure. The stability of the compounds in DMSO is evidenced by the similar absorption characteristics in DMSO (Fig. S6).

The fluorescence spectra of **PyztH**, **1**, **2** and **3** in CH_3OH solution (10^{-5} M) with an excitation wavelength of 370, 380, 390 and 380 nm, respectively, are shown in Fig. 3. The fluorescence emission bands of **PyztH**, **1**, **2** and **3** are observed at 713, 813, 814 and 768 nm, respectively. The fluorescence intensities of **1** and **2** are higher than **PyztH** and **3**. The increase of fluorescence intensity of **PyztH** upon coordination with metal ions proves its good chelating behaviour through charge transfer from the ligand to the metal [41–43]. The nature of the emission spectra indicates that **1** and **2** are more luminescent than **3**. The complexes may be used in photochemical applications due to their fluorescent nature [44].

3.2. X-ray crystallographic structure descriptions of **1**, **2** and **3**

The chemical structures and the synthetic route of **1**, **2** and **3** are given in Scheme 2. Suitable single crystals of **1**, **2** and **3** were obtained by slow evaporation from a mixed methanol/acetonitrile solvent system. The block shaped crystals of **1** (green), **2** (brown) and **3** (deep purple) were sorted for an X-ray study. Perspective ORTEP views of complexes **1**, **2** and **3** are shown in Figs. 4, 6 and 7, respectively. All the crystal parameters, selected bond distances and bond angles are given in Tables 2–4, respectively. The single-crystal structure analysis and BVS calculations (Table S1) of complex **2** confirmed the +III oxidation state of the cobalt ion [27,45]. The complexes have triclinic structures with the space group $P-1$.

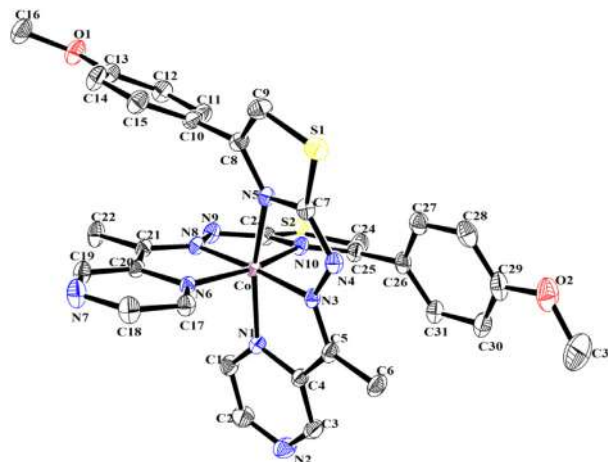


Fig 6. Molecular structure of **2**. Thermal ellipsoids are drawn at the 55% probability label. For the clarity of the structure, hydrogen atoms have been omitted. The structure is truncated to highlight the ligand–metal binding geometry.

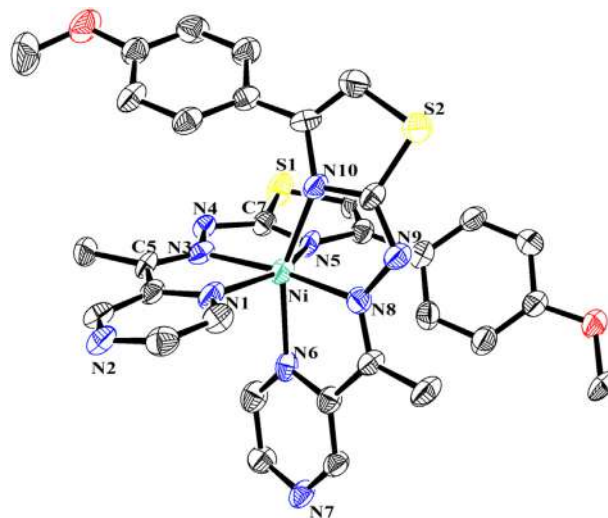


Fig 7. Molecular structures of **3**. Thermal ellipsoids are drawn at the 55% probability level. The structure is truncated to highlight the ligand–metal binding geometry. The hydrogen atoms have been omitted for clarity.

The crystallography data of **1** show that two molecules are present in a unit cell and one is independent of the other molecule in the asymmetric unit. The two molecules in the cell are related by a centre of symmetry. The iron atom is surrounded by two neutral NNN donors (**PyztH**) in an octahedron environment in such a way that the pyrazine (N1, N6), hydrazone (N3, N8) and thiazole (N5, N10) nitrogen atoms of the two ligand units arrange themselves in *trans*, *cis* and *cis* positions. Two bromide ions are present outside of the coordination zone and satisfy the primary valency of the iron(II) ion, as shown in Fig. 4. The X-ray crystal structure shows the complex has a meridional configuration, but it is not a symmetrically octahedral. The dihedral angle between the equatorial plane (N1, N3 and N5) and the axial plane (N6, N8 and N10) is 83.28° , indicating a slight distortion is arising due to steric crowding between the two bulky ligands. The orthogonal bond distances of Fe–N1 and Fe–N6 are the same [1.955(2) Å] as each other. Another two orthogonal bond, Fe–N5 and Fe–N10 *trans* to Fe–N1 and Fe–N6, are also the same [2.012(2) Å] and are slightly longer than the Fe–N1 and Fe–N6 bond distance. The N1–Fe–N3, N6–Fe–N8, N3–Fe–N5 and N8–Fe–N10 bond angles are 79.79, 80.37,

Table 2
Crystallographic data of **1**, **2** and **3**.

Parameter	1	2	3
Formula	C ₃₂ H ₃₀ FeN ₁₀ O ₂ S ₂ Br ₂	C ₃₂ H ₂₈ CoN ₁₀ S ₂ O ₂ PF ₆	C ₃₂ H ₂₈ N ₁₀ NiO ₂ S ₂ , ClO ₄
CCDC No.	1935703	1935712	1935889
Mol. Wt.	882.47	852.66	806.90
Crystal system	Triclinic	Triclinic	Triclinic
Space group	<i>P</i> -1	<i>P</i> -1	<i>P</i> -1
T (K)	150	150	150
a (Å)	11.3805(9)	11.6765(6)	8.480(2)
b (Å)	13.1007(8)	12.4608(7)	12.467(3)
c (Å)	13.3695(8)	12.5849(6)	17.156(5)
α (°)	67.686(2)	95.684(2)	97.296(7)
β (°)	75.725(2)	96.121(2)	94.629(7)
γ (°)	89.222(2)	104.254(2)	106.657(7)
V (Å ³)	1779.96(19)	1749.62(16)	1710.4(8)
Z	2	2	2
D _{calc} (g cm ⁻³)	1.567	1.643	1.619
F(000)	886.29	869.79	831.75
h, k, l (max)	14,16,17	16,17,17	10,15,20
R ₁	0.0350 (6164)	0.0352 (7797)	0.0670 (2982)
WR ₂	0.0932 (7834)	0.0919 (9482)	0.2085
2θ	27.127	29.311	25.328

$$^a R_1 = \sum(|F_o| - |F_c|) / \sum|F_o|.$$

$$^b wR_2 = \left(\sum[w(F_o^2 - F_c^2)^2] / \sum[w(F_o^2)^2] \right)^{1/2}, w = 1 / [\sigma^2(F_o^2) + (0.0265P)^2 - 0.4876P], \text{ where } P = (F_o^2 + 2F_c^2) / 3.$$

80.94 and 80.77°, respectively. Analysis of the crystal packing shows the presence of hydrogen bonds between the H4 and H9 atoms with two Br counter ions, which adds extra stability to the

crystalline state. The hydrogen bond distances of H4···Br2 and H9···Br1 bond are 2.27 and 2.48 Å, respectively, and these are shown in Fig. 5 and Table 5.

In complex **2**, the unit cell contains two molecules. Each cobalt atom is coordinated with two deprotonated ligands, forming an octahedral CoN₆ core (Fig. 6). The primary valency of the complex unit is satisfied by two mono deprotonated ligands and one PF₆⁻ ion, confirming the trivalency of the cobalt ion. The low spin +III oxidation state of the cobalt ion is confirmed by the Co–N bond lengths, being in the range 1.873–1.9504 Å, which are similar to other reported cobalt(III) complexes [22]. Each of the NNN donor ligands forms a five member chelate ring and these are perpendicular to each other. A rigid symmetrical octahedral geometry with the *mer* configuration is formed in **2**. The two outward pointing *cis* pyrazine and *cis* thiazole nitrogen donors are approximately orthogonal to each other and the bond angle between two orthogonal nitrogen atoms of the pyrazine (N1–Co–N6) and the thiazole groups (N5–Co–N10) are 94.35 and 96.25°, respectively (Table 3).

The asymmetric unit cell of **3** (Fig. 7) also contains two molecules. The monomeric structure of the complex exhibits a slightly distorted geometry (meridional arrangement) about the nickel ion. It is to be noted that unlike **1** and **2**, in complex **3** the NiN₆ core has one mononegative (Pyzt⁻) and one neutral ligand (PyztH), where the ligands approach the metal centre perpendicularly. The angle between the equatorial plane N1–N3–N5 and the axial plane N6–N8–N10 is about 90°. The two axial bond distances, Ni–N1 [2.146(7) Å] and Ni–N5 [2.123(7) Å], are slightly elongated compared to the four equatorial bonds, Ni–N3 [2.022(6) Å], Ni–N6 [2.098(6) Å], Ni–N8 [2.003(7) Å] and Ni–N10 [2.087(6) Å] (Table 3). The complex is associated with π–π stacking interactions in the unit cell between the π-electron clouds of two pyrazine moieties,

Table 3
Bond distances of **1**, **2** and **3**.

1		2		3	
Bond Type	Length (Å)	Bond Type	Length (Å)	Bond Type	Length (Å)
Fe–N1	1.955(2)	Co–N1	1.927(2)	Ni–N1	2.146(7)
Fe–N3	1.899(2)	Co–N3	1.886(1)	Ni–N3	2.022(7)
Fe–N5	2.013(2)	Co–N5	1.949(2)	Ni–N5	2.123(6)
Fe–N6	1.950(2)	Co–N6	1.925(1)	Ni–N6	2.098(6)
Fe–N8	1.898(2)	Co–N8	1.884(1)	Ni–N8	2.003(7)
Fe–N10	2.012(2)	Co–N10	1.950(1)	Ni–N10	2.087(6)

Table 4
Bond angles of **1**, **2** and **3**.

1		2		3	
	Angle (°)		Angle (°)		Angle (°)
N1–Fe–N3	79.79(9)	N1–Co–N3	82.50(6)	N1–Ni–N3	76.5(2)
N1–Fe–N5	160.00(9)	N1–Co–N5	164.17(6)	N1–Ni–N5	153.4(2)
N1–Fe–N6	94.19(9)	N1–Co–N6	94.35(6)	N1–Ni–N6	87.5(2)
N1–Fe–N8	94.90(9)	N1–Co–N8	93.88(6)	N1–Ni–N8	96.5(3)
N3–Fe–N5	80.94(9)	N3–Co–N5	81.68(6)	N3–Ni–N5	77.1(2)
N3–Fe–N6	94.88(9)	N3–Co–N6	95.57(6)	N3–Ni–N6	97.7(2)
N3–Fe–N10	103.89(10)	N3–Co–N10	100.17(6)	N3–Ni–N10	107.7(2)
N5–Fe–N8	104.76(9)	N5–Co–N8	101.91(6)	N5–Ni–N8	109.6(2)
N5–Fe–N10	91.96(9)	N5–Co–N10	96.25(6)	N5–Ni–N10	91.7(2)
N6–Fe–N8	80.37(9)	N6–Co–N8	82.80(6)	N6–Ni–N8	77.5(2)
N6–Fe–N10	161.15(9)	N6–Co–N10	164.25(6)	N6–Ni–N10	154.6(2)
N8–Fe–N10	80.77(9)	N8–Co–N10	81.45(6)	N8–Ni–N10	77.4(2)

Table 5
Hydrogen bonds of **1**.

Compound	D–H···A	d(D–H) (Å)	d(H···A) (Å)	d(D···A) (Å)	<DHA (°)	Symmetry
1	N4–H4···Br2	0.87(4)	2.27(4)	3.088(2)	156(3)	1 – x, 1 – y, –z
	N9–H9···Br1	0.79(4)	2.48(4)	3.243(2)	162(4)	

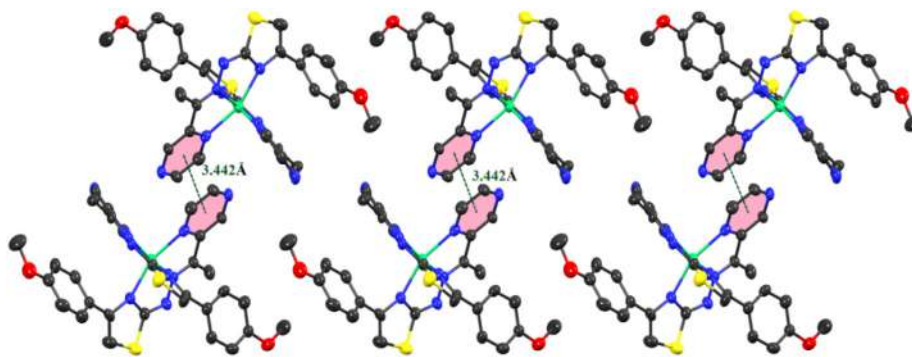


Fig 8. The π - π stacking interactions between pyrazine moieties in the unit cell.

one from a neighbouring molecule. The π - π stacking may help the stability of the complex in the solid state (Fig. 8).

3.3. DFT study and chemical reactivity

The frontier molecular orbitals can be used to estimate the electrical and optical properties, electronic transitions and kinetic stability [46]. The HOMO-1, HOMO, LUMO and LUMO+1 pictures for the complexes, with the energy appended, are given in Fig. 9. The MO orbital picture of **1** shows maximum ligand orbital participation in the MO formation, but the contribution of the metal orbital in the LUMO-1 is higher compare to the HOMO. The π -electron

clouds are delocalized over the thiazole and benzonitrile ring of one ligand in the HOMO-1 and HOMO, and for both ligands in the LUMO and LUMO+1. The contribution of the metal orbital is observed in the MO formation of **2** and **3**, but it is less compared to the participating ligand orbitals, indicating localized electron density over the ligand orbitals. This result implies that the ligands have π -accepting properties, which is also supported by the UV-visible spectra. Chemical descriptors such as softness (S), hardness (η), electronegativity (χ), chemical potential (μ) and electrophilicity (ω) can be investigated using the energy gap ($\Delta E_{\text{HOMO}} - \Delta E_{\text{LUMO}}$) [46-52]. All the calculated values are given in Table 6. The general working formula are:

Complex	HOMO-1	HOMO Energy (eV)	LUMO Energy (eV)	LUMO + 1 Energy (eV)
1				
Energy (eV)	-10.8774	-10.7496	-8.1366	-8.0843
2				
Energy (eV)	-8.1827	-8.0787	-5.6928	-5.6199
3				
Energy (eV)	-10.9768	-10.9051	-9.6750	-8.1451

Fig 9. Frontier molecular orbital picture, HOMO-1, HOMO, LUMO and LUMO+1, of **1**, **2** and **3** with the energy values.

Table 6Calculated E_H , E_L , energy band gap ($E_H - E_L$), chemical potential (μ), electronegativity (χ), global hardness (η), global softness (S) and global electrophilicity index (ω) for **1**, **2** and **3**.

Complex	E_H (eV)	E_L (eV)	$(E_H - E_L)$ (eV)	χ (eV)	M (eV)	H (eV)	S (eV^{-1})
1	-10.7496	-8.1366	-2.631	9.4431	-9.4431	1.3065	0.6532
2	-8.0787	-5.6928	-2.3859	6.8857	-6.8857	1.1929	0.5964
3	-10.9051	-9.6750	-1.2301	10.290	-10.290	0.6150	0.3075

$$\chi \text{ (electronegativity)} = -\frac{1}{2} (E_{LUMO} + E_{HOMO})$$

$$\mu \text{ (potential)} = -\chi = \frac{1}{2} (E_{LUMO} + E_{HOMO})$$

$$\eta \text{ (hardness)} = \frac{1}{2} (E_{LUMO} - E_{HOMO})$$

$$S \text{ (softness)} = \frac{1}{2}\eta.$$

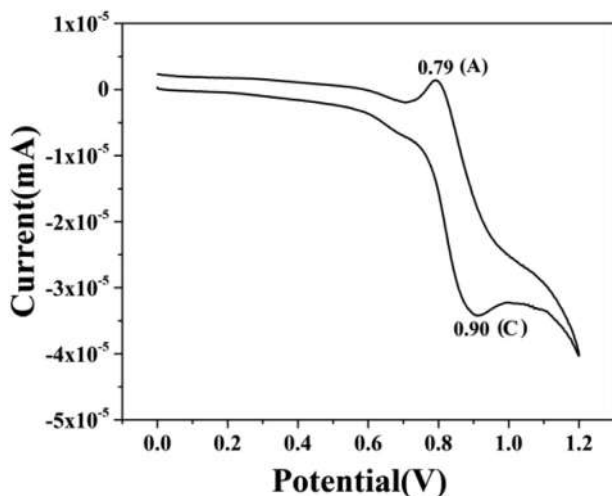
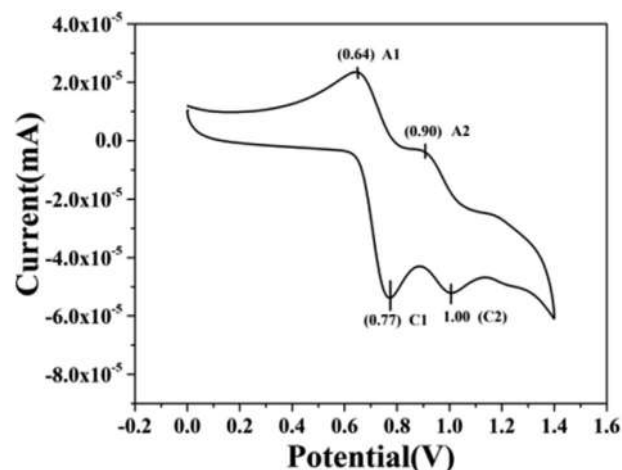
3.4. Cyclic voltammetric study of **1**, **2** and **3**

An electrochemical study of complexes **1**, **2** and **3** was performed in acetonitrile solvent using 0.1 M tetra butyl ammonium perchlorate as a supporting electrolyte at room temperature, using cyclic voltammetry instrument model CHI630E. The electrode potential values are given in Table 7. The cyclic voltammogram of **1** in Fig. 10 shows only one reduction peak at 0.79 V (A) with respect to the Ag/AgCl electrode in saturated KCl, implying that the Fe(III) ion is reduced to the Fe(II) ion in the presence of the ligand environment, and one oxidation peak at 0.90 V (C) with respect to the Ag/AgCl electrode in saturated KCl, indicating the Fe(II) ion is oxidized into the Fe(III) ion in the presence of the applied potential.

The CV of **2** (Fig. 11) shows two reduction peaks at 0.64 V (A1) and 0.90 V (A2) versus Ag/AgCl in saturated KCl, implying that the Co (III) ion is reduced to the Co(II) ion and then the Co(II) ion is reduced to the Co(I) ion, while there are two oxidation peaks at 0.77 V (C1) and 1.00 V (C2), for the reverse process, Co(II) \rightarrow Co(III) and Co(I) \rightarrow Co(II), respectively. The DFT results of complex **2** indicate that the contribution of metal orbitals is comparatively less than that of the ligand orbitals. It is expected that the reduction

Table 7 $E_{1/2}$ values in eV for **1**, **2** and **3**.

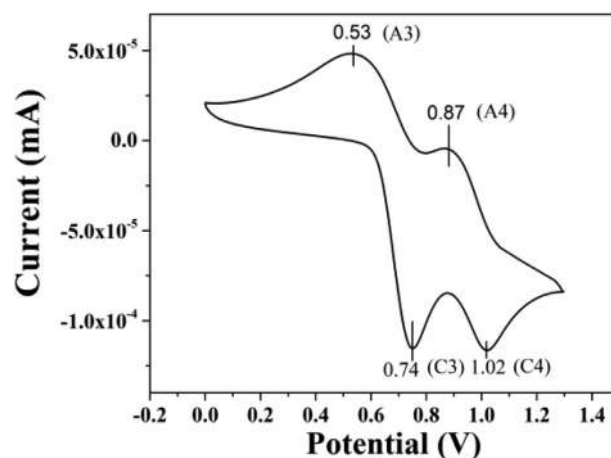
Complex	E_{pA1}	E_{pC1}	$(E_{1/2})^1$	E_{pA2}	E_{pC2}	$(E_{1/2})^2$
1	0.79	0.90	0.85	-	-	-
2	0.69	0.77	0.73	0.94	1.00	0.97
3	0.54	0.74	0.64	0.88	1.02	0.95

**Fig. 10.** Cyclic voltammogram of **1** in acetonitrile containing tetrabutyl-ammonium perchlorate as a supporting electrolyte at a scan rate of 20 mV/s.**Fig. 11.** Cyclic voltammogram of **2** in methanol containing tetrabutyl-ammonium perchlorate as a supporting electrolyte at a scan rate of 20 mV/s.

peaks are mainly due to ligand reduction and the electron transitions occur from the HOMO (ligand) to the LUMO (ligand).

In the complete scan of **3** (Fig. 12) in dry acetonitrile solvent, in presence of tetrabutyl-ammonium perchlorate as a supporting electrolyte, the voltammogram displays two reduction signal A3 and A4, with their corresponding oxidation signals C3 and C4. For the process A3, the half-wave potential ($E_{1/2}$) value is 0.64 V and for process A4, the half-wave potential ($E_{1/2}$) value is 0.95 V. The two reduction peaks, 0.54 (A3) and 0.87 V (A4), correspond to Ni(II) \rightarrow Ni(I) and Ni(I) \rightarrow Ni(0) processes in the presence of the ligand environment.

The CV results thus prove that the complexes undergo quasi-reversible redox processes, which suggest that **2** and **3** might be biologically potent and could influence biological redox processes.

**Fig. 12.** Cyclic voltammogram of **3** in methanol containing tetrabutyl-ammonium perchlorate as a supporting electrolyte at a scan rate of 20 mV/s.

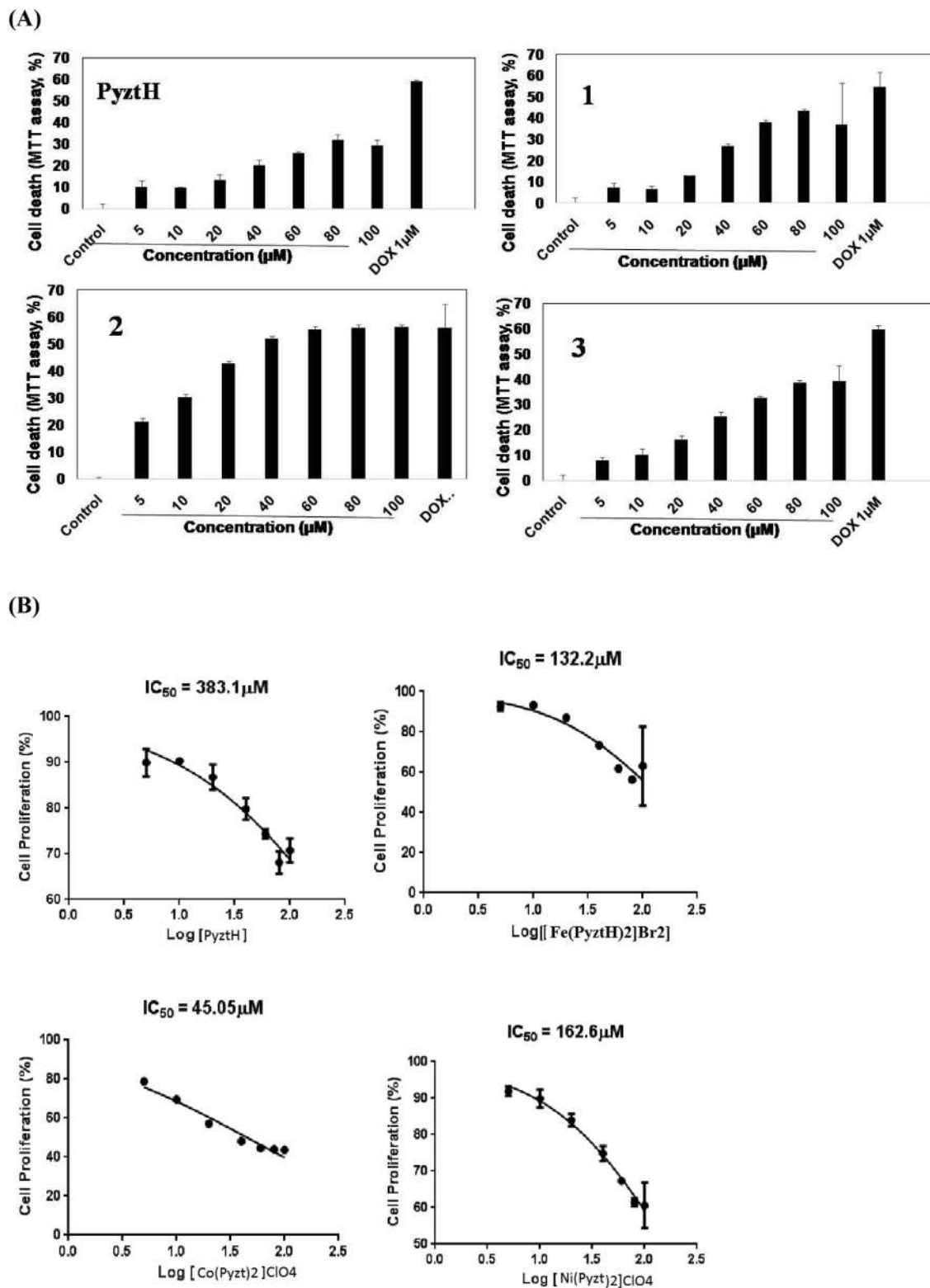


Fig 13. Cytotoxicities of the compounds to U-937 cells. U-937 cells (5000 cell/well for a 96-Well plate) were treated with different concentrations of the ligand (**PyztH**) and its derivatives **1**, **2** and **3** for 72 h in triplicate. The MTT cell viability was assayed. Mean cell death from triplicate samples were calculated as percentages, considering an untreated cell death is 0% and indicated in graph (A). U-937 cells were treated as shown above for 72 h with different concentrations of the ligand **PyztH**, **1**, **2** and **3**; an MTT assay was done and the percentage of the cell viability was plotted in group (B). Data were transformed, normalized and IC_{50} values were calculated using Graph pad Prism. Data represents mean of the three independent experiments.

3.5. Biological activity

3.5.1. Cytotoxicity assay of **PyztH**, **1**, **2** and **3**

U-937 human monocytic cells were treated with **PyztH**, **1**, **2** and **3** to prove their *ex vivo* cytotoxicity using an MTT assay. Complex **2** shows the highest cytotoxic effect against the U937 human monocytic cell line with an IC₅₀ value of 45.11 μM (Fig. 13). The other complexes show relatively less cytotoxicity, having IC₅₀ values of 132 μM (for **1**) and 162.6 μM (for **3**). However, the ligand **PyztH** has the lowest cytotoxicity with an IC₅₀ value of 383 μM. The variations in cytotoxicity depend on the coordination, structure, oxidation state, electronic environment, redox behaviour and lability of the compounds. The structural changes when applied to a cell reveal some interesting trends that may help in the understanding of the structure–activity relationship and further help in optimization of ligands and their derivatives.

The cobalt(III) centre of **2**, having a symmetrical octahedral geometry with a meridian conformation, may readily accept an electron ($E^\circ = 0.64$ V) initiating a favourable electron transfer pathway to generate reactive oxygen species (ROS) from molecular oxygen. The ease of reduction of the Co(III) centre thus causes a higher cytotoxicity effect than any of the other complexes in the group under discussion. It is to be noted that from the reduction potentials, 0.79 V (Fig. 10) and 0.87 V (Fig. 12), it is quite expected that **1** and **3** will be less redox active than the cobalt complex (**2**). A series of cobalt complexes with similar octahedral coordination environments with a CoN₆ core have been shown to have anticancer properties [53]. Other mixed ligand complexes of cobalt (III) were shown to cleave pBR 322 DNA in presence of 3-mercaptopropionic acid and were also effectively cytotoxic towards MCF-7 [54–56].

3.5.2. Lactate dehydrogenase (LDH) release assay

LDH assays were employed to differentiate apoptotic (programmed cell death) activity of these compounds from necrotic activity. We observed that the compounds under investigation exert cytotoxicity in tumor cells. The lactate dehydrogenase (LDH) enzyme, a marker of cytoplasm leakage due to necrosis, was assayed to elucidate the physiological pathway followed by the compounds to elicit their action on the cells when the U-937 human monocytic cell line was treated with **PyztH** and its derivatives **1**, **2** and **3**. The LDH release was measured after 6 and 24 h treatment. The compounds showed a much lower release of LDH as compared to Triton X-100 (100% cell lysis), which displays the necrotic mode of cell death. The compound **1** and **PyztH** showed about 25% LDH release, which is indicative of the necrotic mode of cell death. On the contrary, **2** and **3** showed very little release of LDH, which strongly suggests the occurrence of apoptosis (Fig. 14).

3.5.3. PARP cleavage

Poly (ADP-ribose) polymerase (PARP) is a highly abundant nuclear enzyme which is involved in the DNA repair process; DNA damage activates PARP using NAD⁺ as a substrate to produce

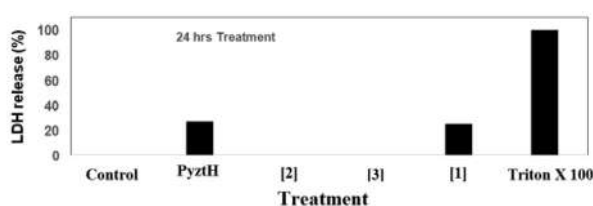
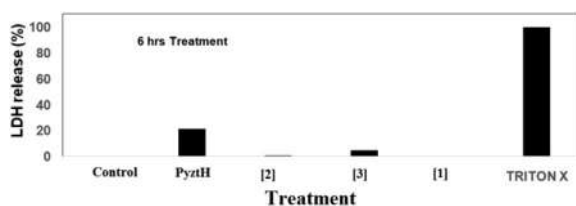


Fig 14. Effect of the compounds on cytolysis of U937 cells. The U937 cells were treated with IC₅₀ values of **PyztH**, **2**, **3** and **1** for 6 and 24 h of treatment. The LDH release was plotted as a percentage against Triton X-100, which is considered as 100% and untreated cells were considered as 0%.

poly ADP ribose. The activation of the apoptosis-specific family of proteases Caspases results in the cleavage of PARP. The cleavage produces the C-terminal 89 kDa fragment which is detected by western blot. The occurrence of an apoptotic mode of cell death is further validated employing *in vitro* PARP cleavage (Fig. 15). Apoptosis nature of **2** was further supported by the appearance of a band of cleaved PARP at 89 kDa at concentrations of 25 μM and 50 μM. The non-appearance of the corresponding bands for **1** and **3** reveals their lower potency than **2**. So, it can be concluded that complex **2** shows the highest antitumor activity following the apoptosis mode of cell death mechanism. This fact is also attested by the low level of the LDH release assay of **2**. It is to be mentioned that **PyztH** showed a 25% LDH release whereas **1** did not show any cleaved PARP band. It is interesting to note that the derivative **3** showed a base level of LDH release, but did not show any sign of PARP cleavage.

Therefore, it can be concluded that although **3** displays cytotoxicity, the activity is somewhat surpassed by that of **2**. In conclusion, cobalt and nickel complexes of pyrazine-thiazole based ligands could be used as effective anticancer agents and in our complexes the activity order will be **2** > **3**.

3.5.4. Screening on PBMCs

The screening was repeated on peripheral blood mononuclear cells (PBMCs) to check the effect of the compounds on the primary cells of the human immune system. As is shown in Fig. 16, the most potent compound is **2**, as revealed by cascade biological experiments with no signature of apoptosis on PBMCs. **PyztH**, **1** and **3** did not show any cytotoxic effect on PBMCs. Thus it is now safe to conclude that **2** is the most efficient antitumor agent in the group under discussion and can be taken for further validation in clinical tests as the said compound has protective and non-toxic properties in the human immune system.

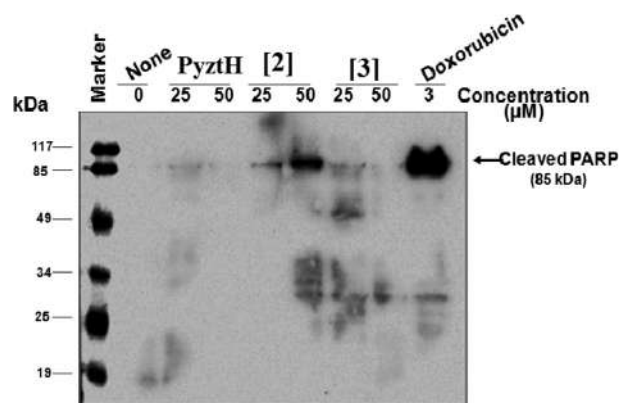


Fig 15. U-937 cells (2×10^6 /mL) were treated with 25 μM and 50 μM concentrations of **PyztH**, **2**, **3** and **1** for 24 h. Whole cell lysate was run on Western blot and probed against the cleaved PARP antibody. Doxorubicin (3 μM) treated cells were used as a positive control.

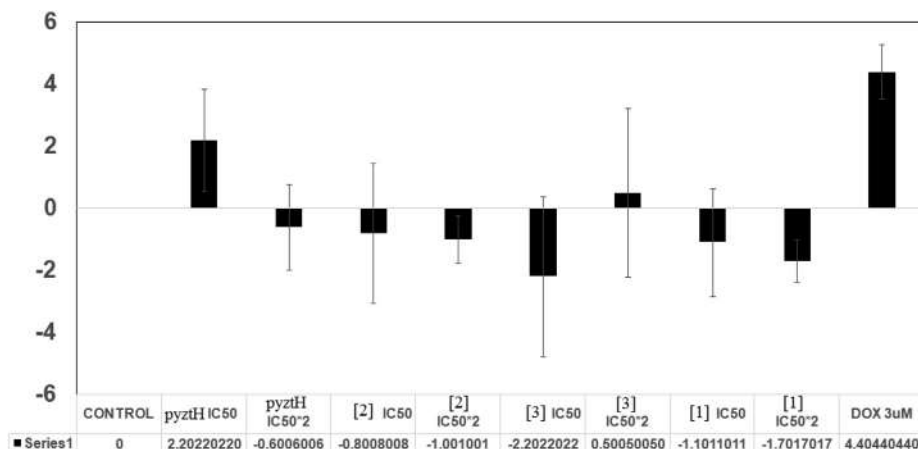


Fig 16. Cytotoxic effect of the ligand PyztH, **2**, **3** and **1** on peripheral blood mononuclear cells (PBMCs). PBMCs (10^4 cells/well) were treated in triplicate with the concentrations of IC50 and IC50 \times 2, each for 24 h. An MTT assay was done and cell death was calculated, considering the value of untreated cells as 0%.

3.5.5. Binding study of PyztH, **1**, **2** and **3** with CT-DNA

3.5.5.1. DNA binding study with a UV-visible spectrophotometer. Metal complexes can bind to DNA via covalent and/or non-covalent interactions. A labile ligand covalently attached to a complex is usually replaced by a nitrogen base of DNA via a covalent interaction, whereas non-covalent DNA interactions include intercalation, electrostatic and groove binding or the stacking of metal complexes along the outside of the DNA helix and grooves. UV-Vis spectroscopy is used to investigate the DNA binding properties of PyztH and its metal complexes (**1**, **2** and **3**) usually Tris buffer (50 mmol Tris-HCl and 50 mmol NaCl) of pH 7.4 is used

as a solvent to perform the DNA binding interaction study. The UV-Vis absorption spectra are changed significantly in the presence of CT-DNA. The absorption spectra of PyztH and its complexes **1**, **2** and **3** with different concentrations of CT-DNA are shown in Fig. 17. The intensity of the MLCT transitions decreases in each sample upon addition of CT-DNA. Prominent hypochromic shifts are observed for PyztH and **3**. The 13.6 and 17.6% hypochromicity for PyztH are observed at 284 ($\pi \rightarrow \pi^*$) and 370 nm ($\pi \rightarrow \pi^*$), respectively, whereas 26.6 and 15.0% hypochromicity for **3** are found at 380 ($\pi \rightarrow \pi^*$) and 505 nm ($d \rightarrow \pi^*$), respectively, with bathochromic shifts. The binding constant k_b is $2.24 \times 10^4 \text{ M}^{-1}$

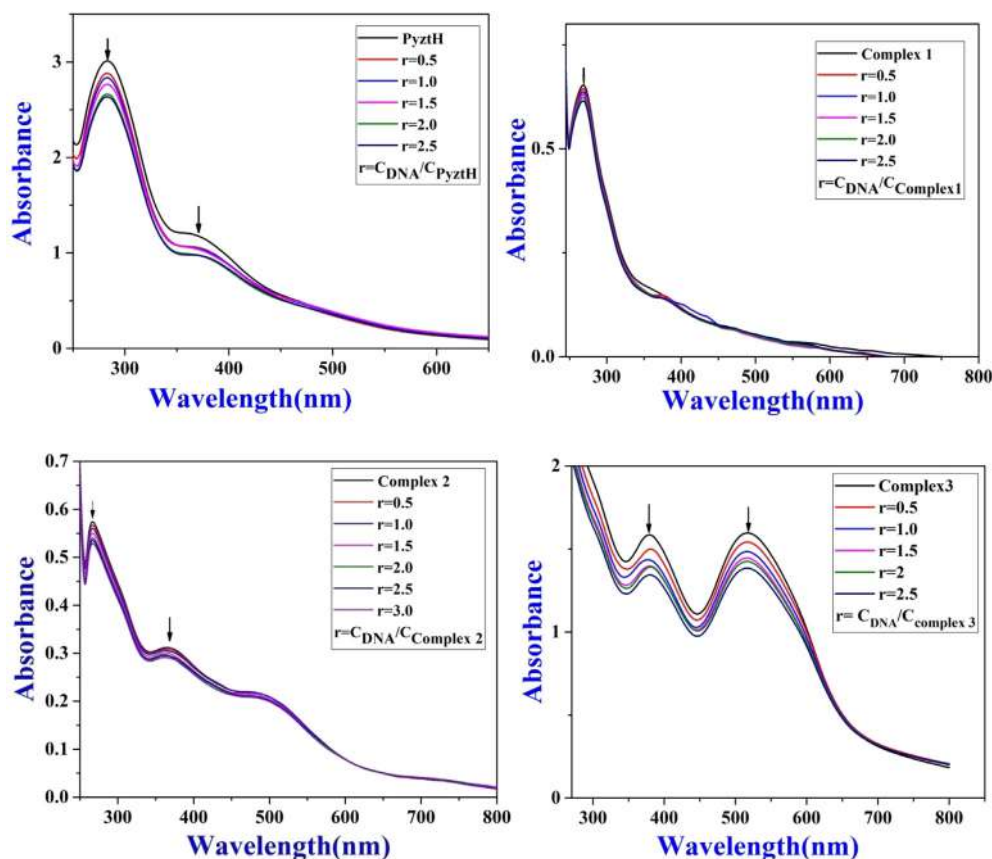


Fig 17. Quenched fluorescence spectra of DNA (50 μM) bound to EB (50 μM) in the absence and presence of increasing concentrations of complexes (0–50 μM) at 350 nm. PyztH, (**1**) Fe(II)-Pyzt and (**2**) Co(III)-Pyzt(**3**) Ni(II)-Pyzt in TrisHCl buffer (pH 7.4) at 25 $^\circ\text{C}$. Arrow (\downarrow) shows the emission intensity decreases upon increasing the concentration of the complexes.

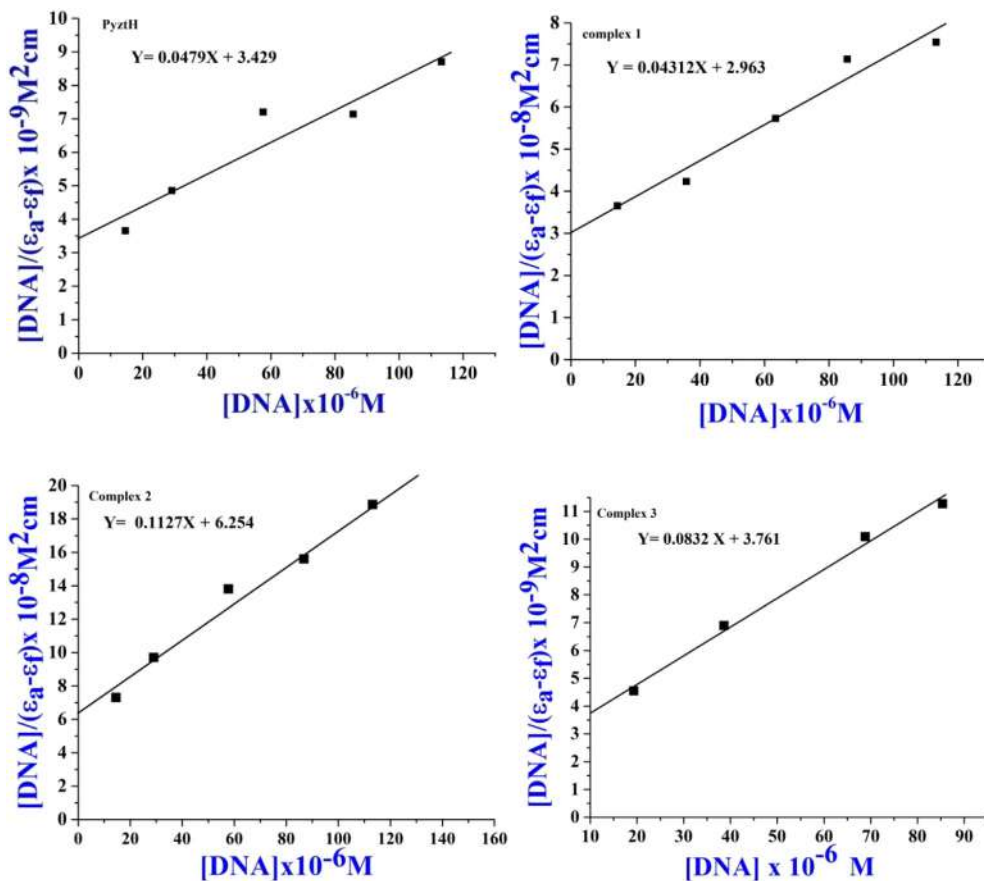


Fig 18. The DNA binding constant was calculated for PyztH and 1, 2 and 3 using linear plot data and the equation $[DNA]/(\epsilon_a - \epsilon_f) = 1/K_b(\epsilon_b - \epsilon_f) + [DNA]/(\epsilon_b - \epsilon_f)$.

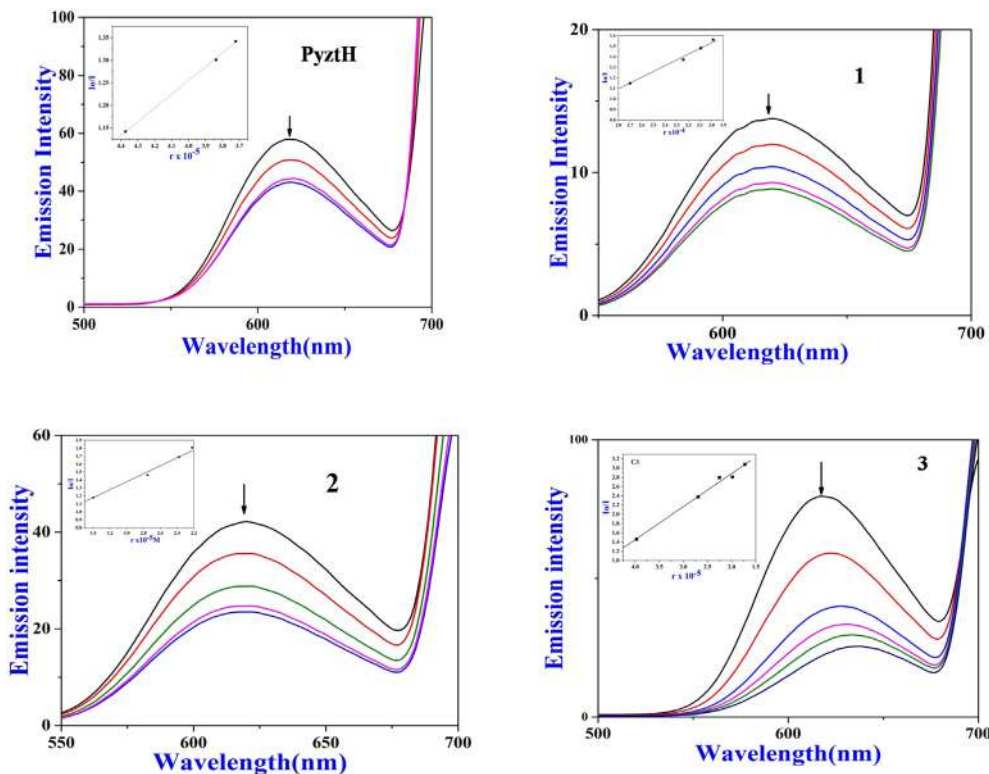


Fig 19. Quenched fluorescence spectra of DNA (50 μM) bound to EB (50 μM) in the absence and presence of increasing concentrations of the complexes (0–50 μM) at 350 nm. PyztH, Fe(II)-Pyzt (1), Co(III)-Pyzt (2) and Ni(II)-Pyzt (3) in TrisHCl buffer (pH 7.4) at 25 °C. Arrow (↓) shows the emission intensity decreases upon increasing the concentration of the complexes.

for **PyztH** and $3.36 \times 10^4 \text{ M}^{-1}$ for **3**, which are indicative of a groove binding property with the base pair of DNA [57,58]. Complex **2** shows hypochromicity for the bands at 358 ($\pi \rightarrow \pi^*$), 441 ($d \rightarrow \pi^*$) and 639 nm (${}^2T_{2g} \rightarrow {}^2E_g$), and the corresponding k_b value is $2.27 \times 10^4 \text{ M}^{-1}$, which is also indicative of a groove binding property. A similar binding property of **1** can be predicted by the observed bathochromic shifts at 303 ($\pi \rightarrow \pi^*$), 373 ($\pi \rightarrow \pi^*$) and 507 nm ($d \rightarrow \pi^*$). The k_b value ($2.5 \times 10^4 \text{ M}^{-1}$) of **1** supports the groove binding interaction with the DNA surface [59]. The binding constant of the corresponding compound with CT-DNA is expressed by the intrinsic binding constant K_b . The constant can be determined by monitoring the absorbance at a fixed wavelength with increasing concentrations of CT-DNA, using the Wolfe-Shimmer equation [59,60].

$$[\text{DNA}] / (\varepsilon_a - \varepsilon_f) = [\text{DNA}] / (\varepsilon_b - \varepsilon_f) + 1 / K_b |(\varepsilon_b - \varepsilon_f)|$$

where $[\text{DNA}]$ is the concentration of DNA, $\varepsilon_a = A_{\text{obsd}} / [\text{complex}]$, $\varepsilon_f =$ the extinction coefficient for the free (unbound) complex and $\varepsilon_b =$ the extinction coefficient for the complex in the fully bound form. A plot of $[\text{DNA}] / (\varepsilon_b - \varepsilon_f)$ vs $[\text{DNA}]$ gives a slope of $[1 / (\varepsilon_b - \varepsilon_f)]$ and the intercept $[1 / K_b (\varepsilon_b - \varepsilon_f)]$, thus the K_b value can be found from the ratio of the slope and the intercept, as shown in Fig. 18. The groove binding interaction was further examined by docking studies.

3.5.5.2. DNA binding study with the fluorescence method using EB indicator. Fluorescence spectroscopy is also an effective method to

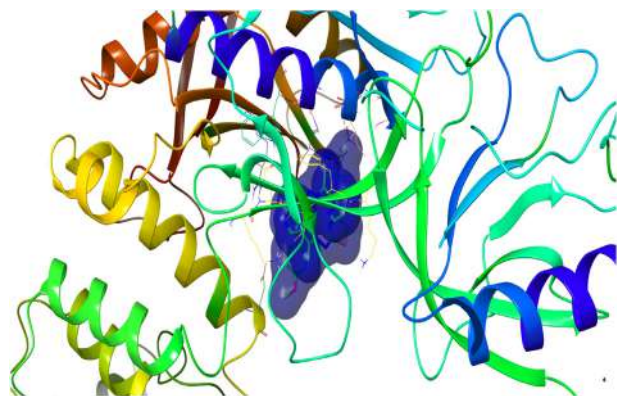


Fig 20. Binding mode of **2** with protein Focal Adhesion Kinase (FAK). The protein is shown in surface, the complex is shown in sticks.



Fig 21. Hydrophobic and hydrogen bond interactions of **2** with Focal Adhesion Kinase (FAK) protein.

determine the binding mode of DNA with metal complexes. A competitive ethidium bromide (EB) binding study has been investigated with the fluorescence spectroscopic titration method in order to investigate the competitive binding nature of the complexes under investigation. The apparent binding constant value of the ligand (**PyztH**) and the complexes are estimated by the fluorescence spectral technique using ethidium bromide (EB) indicator in Tris-HCl/NaCl buffer solution (pH = 7.4) (Fig. 19). In Tris buffer medium, EB is non-emissive due to fluorescence quenching of free EB in the presence of the solvent molecules [57,58]. In the presence of CT-DNA, EB exhibited an enhance emission intensity due to its binding with DNA. A relative binding of **PyztH** and its metal complexes **1**, **2** and **3** to DNA can result in displacement of bound EB or emission quenching, resulting in a decrease of its emission intensity. The quenching constant is calculated using the Stern-Volmer equation $I_0/I = 1 + K_{SV}[r]$ where, I_0 and I are the fluorescence intensities in the absence and presence of the complexes, respectively, K_{SV} is the Stern-Volmer constant and $[r]$ is the concentration of the compound [59]. The apparent binding constants are obtained from the equation $K_{\text{app}} \times [\text{complex}]_{50} = K_{\text{EB}} \times [\text{EB}]$, where K_{app} is the apparent binding constant of the complex, $[\text{complex}]_{50}$ is the concentration of the complex at 50% quenching of DNA-bound EB emission intensity, K_{EB} is the binding constant of EB (where $K_{\text{EB}} = 1.0 \times 10^7 \text{ M}^{-1}$) at a concentration of 1.3 μM (EB) [60]. The low values of binding constant of the ligand **PyztH** and the corresponding complexes **1**, **2** and **3** reveal that the methyl and 4-methoxy phenyl groups attached to pyrazine and thiazole ring, respectively, perpendicular to the binding plane of complexes, probably inhibit the intercalation process with DNA [61–63].

3.5.6. Molecular docking analysis

The docking technique uses computer modelling to visualize the binding mode and interaction between a complex and DNA for rational drug design [64]. The energetically most favourable binding mode and interaction with the protein surface model of representative complex **2** are shown in Figs. 20 and 21, respectively and complexes **1** and **3** are shown in Figs. S7–S10. The docking picture indicates that the complexes are well fitted in the active pocket of the protein chain. The free binding energies of **1**, **2** and **3** are 5.55, 5.45, 5.41 Kcal/mol, respectively. Complex **2** shows a hydrophobic interaction with ASN339, GLU93, GLU94, VAL95, GLU256 and THR335 base pairs and one hydrogen bonding interaction with CYS257 of the protein chain. Hydrophobic interactions are also found in **1** and **3**. The docking parameters suggest that the cobalt complex **2** shows the highest interaction with protein

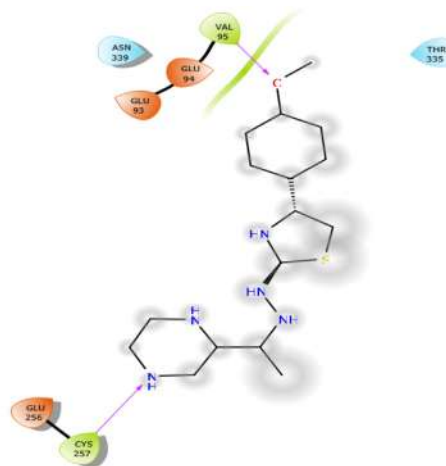


Table 8
Docking results of **Pyzth**, **1**, **2** and **3** (kcal/mol) with protein Focal Adhesion Kinase (FAK).

Compound	vdW + H bond + dissolving energy ($\Delta G_{vdW+hb+desolv}$)	Electrostatic Energy (ΔG_{elec})	Total Internal energy (ΔG_{total})	Torsional Free energy (ΔG_{tor})	Unbound system's energy (ΔG_{unb})	Binding Free energy ($\Delta G_{binding}$)
1	-6.65	-0.09	-2.84	+1.19	-2.84	-5.55
2	-6.47	-0.18	-2.61	+1.19	-2.61	-5.45
3	-6.39	-0.22	-2.98	+1.19	-2.98	-5.41

6cb0 in the group (Table 8). The docking study also attests the best anticancer activity among the tested metal complexes.

4. Conclusion

New pyrazine-thiazole based Fe(II), Co(III) and Ni(II) complexes have been synthesized and characterized by single crystal X-ray analysis, cyclic voltammetry, DFT and spectroscopic techniques. The complexes are non-hygroscopic, air stable and thermally stable up to 200 °C. The cyclic voltammetry study reveals the quasi-reversible nature of the redox reactions. All three complexes crystallize in a similar fashion with the space group *P*-1. The metal centre in each case is octahedrally surrounded by an N6 chromophore. The structures of **1** and **3** have strong hydrogen bonding and π - π stacking interactions, respectively. The compounds show antitumor activity against U-937 human monocytic cells in the order **2** > **3** > **1**. Additionally, in vitro PARP cleavage experiments establish the apoptosis mode of cell death by the cobalt complex (**2**). The binding constants values of the complexes to DNA clearly indicate the groove binding property of the complexes. A molecular docking study proves a significant interaction with the DNA base pair and the best interaction is shown by **2**. Finally, the present study will help to design novel compounds having a pyrazine-thiazole backbone as anticancer and antimicrobial agents for future therapeutics.

Conflicts of interest

There are no conflicts of interest to declare.

Acknowledgement

We gratefully acknowledge the Council for Scientific and Industrial Research (CSIR), Government of India for financial support [grant no. 1(2858)/16/EMR-II]. Panskura Banamali College acknowledges the grants received from Department of Science and Technology (DST), Govt. of India through the FIST program (No.SR-FIST-COLLEGE-295-dt18/11/2015). Also, thanks are given to all members of CRNN, Kolkata and IEST, Shibpur for help in the characterizations.

Appendix A. Supplementary data

Supplementary data to this article can be found online at <https://doi.org/10.1016/j.poly.2020.114503>.

References

- [1] C.W. Bird, *Tetrahedron* 41 (1985) 1409.
- [2] E.F.V. Scriven, C.A. Ramsden, *Heterocyclic Chemistry in the 21st Century* 121 (2017) 1–302.
- [3] K.S. Jain, *Curr. Top. Med. Chem.* 16 (2016) 2839.
- [4] M.T. Chhabria, S. Patel, P. Modi, P.S. Brahmikshatriya, *Curr. Top. Med. Chem.* 16 (2016) 2841.
- [5] S. Karamthulla, S. Pal, Md.N. Khan, L.H. Choudhury, *RSC Adv.* 4 (2014) 37889.
- [6] K.M. Wei, S. Wei, S.B. Tsogoeva, *Org. Biomol. Chem.* 9 (2011) 3457.
- [7] R.M. Mohareb, R.A. Ibrahim, W.W. Wardakhan, *Med. Chem. Res.* 25 (2016) 2187.
- [8] H. Elshafly, S. Bjelogrić, C.D. Muller, T.R. Todorovic, M. Rodic, A. Marinkovic, N. R. Filipovic, *J. Coord. Chem.* (2016) 3354–3366.
- [9] S. Sandhaus, R. Taylor, T. Edwards, A. Huddleston, Y. Wooten, R. Venkatraman, R.T. Weber, A. González-Sarrias, P.M. Martin, P. Cagle, Y.-C. Tse-Dinh, S.J. Beebe, N. Seeram, A.A. Holder, *Inorg. Chem. Commun.* 64 (2016) 45–49.
- [10] M. Schiedel, T. Rumpf, B. Karaman, A. Lehoczky, J. Oláh, S. Gerhardt, J. Ovádi, W. Sippl, O. Einsle, M.J. Zung, *J. Med. Chem.* 59 (2016) 1599–1612.
- [11] G. Poli, Di R. Fabio, L. Ferrante, V. Summa, M. Botta, *Chem. Med. Chem.* 12 (2017) 1917–1923.
- [12] S. Bondock, T. Naser, A.Y. Ammar, *Eur. J. Med. Chem.* 62 (2013) 270–279.
- [13] R.P. Karuvalam, K.R. Haridas, S.K. Nayak, T.N. Guru, P. Rajeesh, R. Rishikesan, N. S. Kumari, *Eur. J. Med. Chem.* 49 (2012) 172–182.
- [14] A. Ozdemir, T.Z. Gulhan, Z.A. Kaplançikl, G. Revial, K. Guven, *Euro. J. Med. Chem.* 42 (2007) 403–409.
- [15] R.R. Gupta, M. Kumar, *Heterocycles* 2 (1999) 416.
- [16] R.M. Mohareb, R.A. Ibrahim, W.W. Wagnat, *Bull. Chem. Soc. Ethiop.* 32 (2) (2018) 259–270.
- [17] W. Cai, R. Ratnayak, M.H. Gerber, Q.Y. Chen, Y. Yu, H. Derendorf, J.G. Trevino, L. Hendrik, *Invest. New Drugs* 37 (2019) 364–374.
- [18] T.D.S. Silva, L.M. Bomfim, A.C.B.C. Rodrigues, R.B. Dias, C.B.S. Sales, C.A.G. Rocha, M.B.P. Soares, D.P. Bezerra, M.V.O.C. Cardoso, A.C.L. Leite, G.C.G. Militão, *Toxicol. Appl. Pharmacol.* 329 (2017) 212–223.
- [19] N. Farrell, L.F. Povirk, Y. Dange, G.D. Masters, M.S. Gupta, G. Kohlhausen, Q.Y. Khan, D.A. Gewirtz, *Biochem. Pharmacol.* 68 (2004) 857–866.
- [20] L.M.T. Frija, A.J.L. Pombeiro, M.N. Kopylovich, *Coord. Chem. Rev.* 308 (2016) 32–55.
- [21] R. Sharma, F.R. Xavier, K.K. Vasu, S.C. Chaturvedi, S.S. Pancholi, *J. Enzyme Inhib. Med. Chem.* 24 (2009) 890–897.
- [22] P. Bera, P. Brandão, G. Mondal, H. Jana, A. Jana, A. Santra, P. Bera, *Polyhedron* 134 (2017) 230–237.
- [23] B. Bertrand, J. Fernandez-Cestau, J. Angulo, M.D. Cominetti, Z.E. Waller, M. Searcey, M.A.O. Connell, M. Bochmann, *Inorg. Chem.* 56 (2017) 5728–5740.
- [24] M.X. Li, D. Zhang, L.Z. Zhang, J.Y. Niu, B.S.Z. Ji, *Organomet. Chem.* 696 (2011) 852–858.
- [25] M.X. Li, D. Zhang, L.Z. Zhang, J.Y. Niu, B.S.Z. Ji, *Eur. J. Med. Chem.* 46 (2011) 4383–4390.
- [26] J. Bostrom, K. Berggren, T. Elebring, P.J. Greasley, M. Wilstermann, *Bioorg. Med. Chem.* 15 (2007) 4077–4084.
- [27] G.M. Sheldrick, *Acta Cryst. A* 71 (2015) 3–8.
- [28] G.M. Sheldrick, *Acta Cryst. C* 71 (2015) 3–8.
- [29] R.G. Parr, W. Yang, *Density Functional Theory of Atoms and Molecules*, Oxford University Press, Oxford, 1989.
- [30] A.D. Becke, *J. Chem. Phys.* 98 (1993) 5648.
- [31] C. Lee, W. Yang, R.G. Parr, *Phys. Rev. B* 37 (1998) 785.
- [32] A.D. Becke, *J. Chem. Phys.* 97 (1992) 9173.
- [33] P. Bera, P. Brandão, G. Mondal, H. Jana, A. Jana, A. Santra, R.B. Mokhamatam, S. K. Manna, T.K. Mandal, P. Bera, *Polyhedron* 159 (2019) 436–455.
- [34] W.N. Burnette, *Anal. Biochem.* 112 (1981) 195–203.
- [35] M. Blot, P. Mahony, *Anal. Biochem.* 247 (1997) 185–192.
- [36] J.M. Brenchley, D.C. Douek, *Methods Cell Biol.* 75 (2004) 481–496.
- [37] S.F. Sousa, P.A. Fernandes, M.J. Ramos, *Proteins: Struct. Funct. Bioinformatics* 65 (2006) 15–26.
- [38] H. Park, J. Lee, S. Lee, *Proteins: Struct. Funct. Bioinformatics* 65 (3) (2006) 549–554.
- [39] Zhong-Lu You, Yong-Ming Cui, Yu-Ping Ma, Che Wang, Xiao-Shuang Zhou, Kun Li, *Inorg. Chem. Commun.* 14 (2011) 636–640.
- [40] I. Mohra, A. Prescimone, D. Haussinger, C.E. Housecroft, E.C. Constable, *RSC Adv.* 9 (2019) 13646–13657.
- [41] V.G. Vaidyanathan, B.U. Nair, *J. Inorg. Biochem.* 94 (2003) 121–126.
- [42] G. Vellaiswamy, S. Ramaswamy, *J. Fluoresc.* 27 (2017) 1559–1565.
- [43] R. Shanmugakala, P. Tharmaraj, C.D. Sheela, C. Anitha, *Int. J. Inorg. Chem.* 2012 (2012) 1–7.
- [44] A. Majumder, G.M. Rosair, A. Mallick, A.N. Chattopadhyay, S. Mitra, *Polyhedron* 25 (2006) 1753–1762.
- [45] M. Dolai, M.J. Ali, *Chem. Sci.* 126 (2014) 1647–1653.
- [46] F.R. See, R.A. Cruse, W.M. Strub, *Inorg. Chem.* 37 (1998) 5369–5375.
- [47] K. Fukui, T. Yonezawa, C. Nagata, H. Shingu, *J. Chem. Phys.* 22 (1954) 1433.
- [48] N. Ozdemir, S. Dayan, O.M. Dinçer, N.O. Kalaycıoğlu, *Mol. Phys.* 111 (2013) 707.
- [49] R.G. Parr, W. Yang, *Density-Functional Theory of Atoms and Molecules*, in *International Series of Monographs on Chemistry*, vol. 16, Oxford University Press, New York, 1989.
- [50] R.G. Parr, L.V. Szentpaly, S. Liu, *J. Am. Chem. Soc.* 121 (1999) 1922–1924.
- [51] J. Janak, *Phys. Rev. B* 18 (1978) 7165.

- [52] J.P. Perdew, R.G. Parr, M. Levy, J.L. Balduz, *Phys. Rev. Lett.* 49 (1982) 1691.
- [53] B.Y.K. Law, Y.Q. Qu, S.W.F. Mok, H. Liu, W. Zeng, Y. Han, F.G. Martinez, W.K. Chan, K.M.C. Wong, V.K.W. Wong, *Oncotarget* 8 (2017) 55003–55502.
- [54] V. Thanilarasan, N. Sengoltuvelan, A. Sudha, P. Srinivasan, G. Chakkaravarathi, *J. Photo. Chem. Photobiol.* 162 (2016) 558–569.
- [55] E.I. Abu, G.M.A.E. Reash, E.O.A. Gammal, S.E. Ghazy, A.H. Radwan, *Spectrochim. Acta. A* 104 (2013) 26.
- [56] A.A.E. Sherif, A. Fetoh, Y.K. Abdulhamed, G.M.A.E. Reash, *Inorg. Chim. Acta* 480 (2018) 1.
- [57] M. Waring, *J. Mol. Biol.* 13 (1965) 269.
- [58] J.B. LePecq, C. Paoletti, *J. Mol. Biol.* 27 (1967) 87.
- [59] K. Sudeepa, N. Narsimha, B. Aparnab, S. Sreekanth, A.V. Aparna, M. Ravib, J. Mahadeb, C. Devi, *J. Chem. Sci.* 130 (2018) 52.
- [60] A.K. Patra, T. Bhowmick, S. Roy, S. Ramakumar, A.R. Chakravarty, *Inorg. Chem.* 48 (2009) 2932.
- [61] S. Sarkar, A. Mondal, D. Chopra, J. Ribas, K.K. Rajak, *Eur. J. Inorg. Chem.* (2006) 3510–3516.
- [62] J. Chen, X. Wang, Y. Shao, J. Zhu, Y. Zhu, Y. Li, Q. Xu, Z. Guo, *Inorg. Chem.* 46 (2007) 3306–3312.
- [63] A. Dimitrakopoulou, C. Dendrinou-Samara, A.A. Pantazaki, M. Alexiou, E. Nordlander, D.P. Kessissoglou, *J. Inorg. Biochem.* 102 (2008) 618–628.
- [64] Z. Zhao, J. Zhang, S. Zhi, W. Song, J. Zhao, *J. Inorg. Biochem.* 197 (2019) 110696.